Macromolecules

pubs.acs.org/Macromolecules Article

Effects of Geometric Confinement on Caging and Dynamics of Polymer-Tethered Nanoparticle Suspensions

Xiaotun Liu, Nyalaliska W. Utomo, Qing Zhao, Jingxu Zheng, Duhan Zhang, and Lynden A. Archer*

Cite This: *Macromolecules* 2021, 54, 426–439 Read Online

ACCESS | Metrics & More | Article Recommendations | Supporting Information

ABSTRACT: Well-dispersed polymer-tethered silica nanoparticles exhibit soft glassy rheology and caging behaviors due to chain interpenetration driven by entropic attraction and geometric confinement. In this study, we use small-angle X-ray scattering and rheology to investigate caging dynamics of silica nanoparticles densely grafted with poly(ethylene glycol) methyl ether (mPEG) dispersed in PEG oligomers (mPEGm). By systematically varying the volume fraction, ϕ_c, of the silica cores in mPEGm hosts, we are able to manipulate the extent of geometric confinement and, by means of vibrational spectroscopy (infrared and Raman), probe how molecular chain conformations are influenced by tethering and confinement. Rheological measurements reveal that the hairy particle suspensions manifest soft glassy dynamics, analogous to those reported in solvent-free hairy nanoparticles, down to particle volume fractions as low as 0.065. A simple geometric model is proposed to explain the emergence of caging and soft glassy rheology of the materials. We show that this model correctly explains the low yield strains observed in the materials and may also be used to rationalize the disappearance of yielding at $\phi_c < 0.065$. Within the soft glassy regime, the hairy nanoparticle suspensions exhibit a peculiar flow curve with an upturn at a low shear rate. And, stress relaxation experiments show a significant unrelaxable stress upon flow cessation. Spectroscopic analysis suggests that tethered PEG chains adopt more trans conformations compared to untethered chains, providing molecular evidence of confinement-induced chain interpenetration in hairy nanoparticle soft glasses.

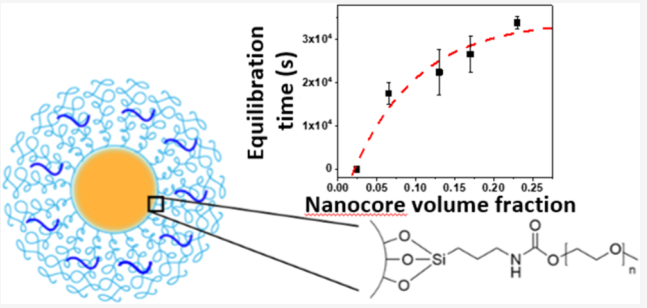

INTRODUCTION

Soft glassy materials, such as foams, emulsions, colloidal suspensions, and star polymer solutions, have gathered appreciable attention over the past few decades. These materials exhibit a distinct yield stress and jamming behaviors as the material elements are confined by proximity to their neighbors, such that they can only exhibit liquid behavior when the applied stress is higher than a critical value termed the yield stress. Understanding the origins of these behaviors has emerged as the subject of both academic[1−12] and practical interest in soft glasses for advanced coating, rheology modifiers, energy storage, and as thixotropic materials.[13−22] As a subclass of the universal class of soft glasses, hairy particles composed of SiO_2 nanostructures that are either ionically or covalently tethered with polymer chains provide opportunities for studying caging, yielding, and jamming of soft glasses in detail.

Multiple, generic features of the soft glassy materials are captured using Sollich's soft glassy rheology (SGR) model.[23,24] According to this model, dynamical elements that constitute the soft glass are trapped in a potential energy landscape formed by their neighbors that does not permit thermally activated relaxation. As a consequence, the materials must rely on the elastic energy stored upon local deformation, to yield and flow. Previous studies of solventless/self-suspended hairy nanoparticles have observed that many of the generic attributes of the materials are consistent predictions of the simple SGR model,[25−31] but that the noise temperature, $X = 1 + 2\delta/\pi$, which describes the effective thermal energy available for the material elements to hop out of the cages that trap them, is a function of the thermodynamic temperature—indicating that the cages themselves are dynamics objects, driving by the underlying relaxation dynamics of molecules that form them. Here, $\tan(\delta) = G''/G'$ is the loss tangent deduced from shear rheology measurements at strains below the yield strain. The material properties of the solventless hairy SiO_2 nanoparticles were also reported to have a synergistic dependence on nanoparticle core size, grafting density, and tethered polymer molecular weight. This effect can be captured in the dynamic properties of the materials by relating them to the volume fraction ϕ_c of the SiO_2 nanoparticle cores. At low polymer content, the viscosity of the materials diverges at a core volume

Received: June 22, 2020
Revised: November 11, 2020
Published: December 16, 2020

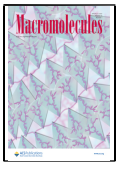

https://dx.doi.org/10.1021/acs.macromol.0c01448
Macromolecules 2021, 54, 426−439

fraction $\phi_c \approx \phi^*_c$ much lower than that for typical colloidal suspensions.[32] At high polymer content, however, the materials may unjam and manifest Newtonian fluid characteristics.[25]

Recently, we reported that self-suspended hairy nanoparticles undergo a significant equilibration process, wherein the interparticle correlations and the caging are substantially enhanced in time.[33] The process was explained in terms of migration of tethered polymer chains toward their more interpenetrated equilibrium states. A simple geometric model for the particles in which crowding and geometric confinement of the particles produces caging of the cores was found to capture the structural and rheological behaviors of the materials, including predicting yield strain values comparable to experimental literature results. Here, we wish to explore this model further by examining the relative roles of crowding and geometric confinement on caging and yielding.

The hairy nanoparticles in this study feature a covalent tethering between the polymer and nanoparticle, which precludes any potential chain dissociation due to impurities such as water and salts as might be possible with ionic tethering. Previous study on SiO_2-PEG/SiO_2-PMMA self-suspended hairy nanoparticle blends reported substantially enhanced interparticle correlations compared to neat hairy nanoparticles due to the favorable interaction between poly(ethylene glycol) (PEG) and poly(methyl methacrylate) (PMMA), as signified by a negative Flory−Huggins interaction parameter.[26] The results suggest that the enthalpic interactions can play a significant role in the material properties of hairy nanoparticles. Here, we would like to exclude any role of such interactions and choose an oligomer solvent of the same chemistry as the tethered chains with end group functionality unable to form hydrogen bonds.

In addition to the established measures to interrogate the caging, we follow the recent study by Lin et al.,[34] where shear reversal experiments were used to decouple frictional and hydrodynamic contributions to the stress tensor in concentrated colloidal suspensions and adapt this procedure to explore the microscale mechanical aspects of the cages formed in hairy nanoparticle suspensions. In this approach, materials were subjected to a specified shear rate to reach steady state, followed by a sudden reverse in shearing direction. The idea is that immediately upon shear reversal, frictional/contact stress immediately decays and develops over time to steady state, whereas the hydrodynamic contribution maintains the same magnitude but instantaneously changes in sign. Here, we develop a simple modification of the procedure in which we apply a shear-rest-shear-reverse process to decouple the various contributions to the stress in jammed materials. We observe that the stress in the hairy nanoparticle soft glasses can be separated into dynamic and static contributions, which correspond to the liquid and solid characteristics, respectively. The static contribution exists as a nonrelaxable residual stress in the materials upon flow cessation even upon a prolonged time scale, which likely reflects the orientations of the interpenetrated sections of the tethered chains comprising the cages. The dynamic contribution, however, appears to reflect the molecular friction from the relative motions of the chains and increases as the shear rate increases.

We study the effects of geometric confinement on the caging dynamics of hairy nanoparticle systems by adding PEG oligomers to alleviate the extent of confinement and observe that caging behaviors such as the cage equilibration, yielding transition, and reformed cage dynamics retain down to some critical ϕ_c^*. We report a flow curve with an upturn at a low shear rate in soft glassy materials, which implies that shear banding occurs in the materials at low shear rates. We also separated the stress contributions in the hairy nanoparticles, showing a significant residual stress potentially reflecting the structure of the cages. We identified that geometric confinement is likely the microscopic origin of caging in hairy nanoparticle systems, with additional implications from infrared and Raman results on chain conformations. In so doing, we develop a comprehensive understanding of the underlying physics in generic hairy nanoparticle systems.

EXPERIMENTAL METHODS

Materials. Silica nanoparticles (LUDOX SM30, 10 ± 2 nm), poly(ethylene glycol) monomethyl ether (mPEG-OH) with M_n = 5000 Da, poly(ethylene glycol) dimethyl ether (mPEGm) with M_n = 500 Da, 3-(triethoxysilyl)propyl isocyanate, 1,4-diazabicyclo [2.2.2.]-octane (DABCO), and anhydrous dichloromethane were purchased from Sigma-Aldrich. The mPEG-OH and mPEGm were dried in vacuo overnight at room temperature before use. All other reagents were used as received.

The synthesis of PEG-tethered silica nanoparticles has been previously reported.[33] The mPEG-OH (M_n = 5000 Da) (10.0 g, 2.00 mmol, 1.00 equiv), 3-(triethoxysilyl)propyl isocyanate (0.495 g, 2.00 mmol, 1.00 equiv), and DABCO (0.336 g, 3.00 mmol, 1.50 equiv) were dissolved in anhydrous dichloromethane (10 mL) and heated to 50 °C for 48 h. The reaction mixture was precipitated into excess hexanes and the mPEG-silane product was isolated by decantation, dried in vacuo at room temperature, and stored at 2−8 °C prior to use.

The silica nanoparticles (LUDOX SM30, 10 ± 2 nm) (1.20 mL) were diluted in excess deionized water (400 mL) and a solution of triethoxysilane-functionalized mPEG (2.00 g) from the previous step in deionized water (50 mL) was dropwise added. The reaction mixture was bubbled with argon and heated to 70 °C for 48 h. The mixture was subsequently dried in a convection oven at 45 °C to remove bulk water and further purified by repeated precipitation into a 1:4 (v/v) mixture of chloroform/hexanes, followed by centrifugation at 8500 rpm to remove untethered chains. The resultant self-suspended hairy nanoparticles were dried partially in a convection oven at 45 °C and more thoroughly in vacuum at room temperature before storage under an argon atmosphere. By altering the ratio of SiO_2 nanoparticles to the triethoxysilane-functionalized mPEG, the grafting density can be manipulated to a degree, and through it the volume fraction of SiO_2 nanoparticles can be varied. Blending the hairy SiO_2-mPEG particles with unfunctionalized PEG chains provides an additional degree of freedom in creating hairy particle suspensions in which the interparticle separation can be systematically adjusted to understand the effect of geometric confinement on physical and dynamic properties of the materials.

A schematic of the hairy nanoparticle suspensions used in the study is illustrated in Figure 1. The suspensions were obtained by dispersing the self-suspended hairy nanoparticles with SiO_2 nanocore volume fraction ϕ_c = 0.23 in deionized water added with different amounts of

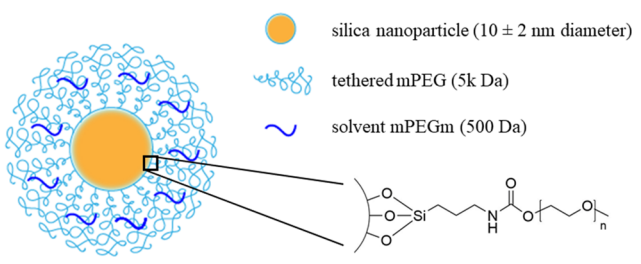

Figure 1. Schematic of the hairy nanoparticle/oligomer suspensions used in the study.

https://dx.doi.org/10.1021/acs.macromol.0c01448
Macromolecules 2021, 54, 426−439

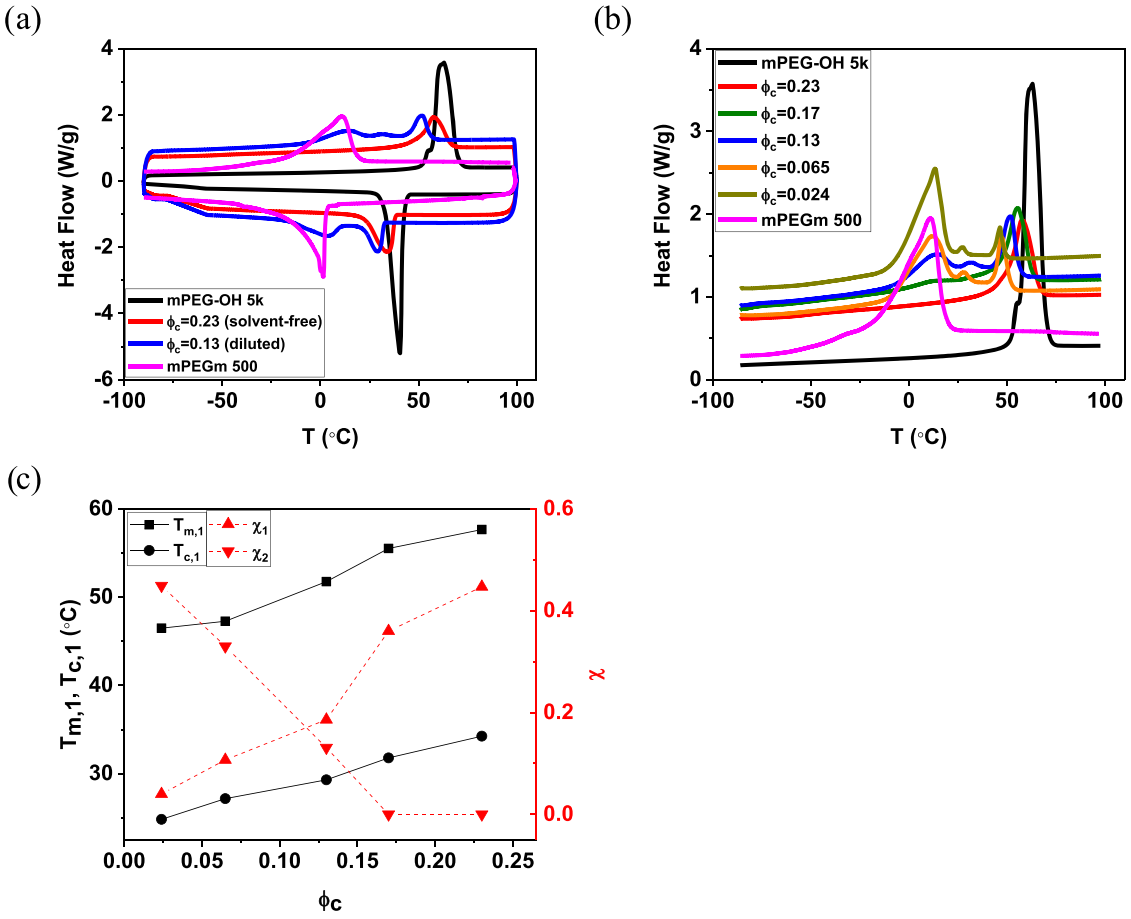

Figure 2. Heat flow as a function of temperature at 10 °C/min for (a) solvent-free hairy nanoparticles and a hairy nanoparticle suspension (heating and cooling cycles) and (b) hairy nanoparticle suspensions in various dilutions (heating cycle) in comparison with untethered PEG (5k Da) chains and oligomer solvent (500 Da). (c) Melting and recrystallization transitions associated with PEG (5k Da) chains and crystallinity associated with PEG (5k Da) (subscript 1) and oligomer solvent (500 Da) (subscript 2) as a function of the core volume fraction of hairy nanoparticle suspensions.

the mPEGm (500 Da) oligomer to adjust the ϕ_c of the ultimate suspensions. The suspensions were ultrasonicated at room temperature for 1 h to fully disperse the SiO_2-PEG/mPEGm mixture, dried in a convection oven at 45 °C to remove bulk water, and dried thoroughly in a vacuum oven at room temperature before storage under an argon atmosphere.

Thermal Analysis. The inorganic content of the polymer-tethered, hairy SiO_2-PEG nanoparticles and their suspensions was estimated using thermogravimetric analysis (TGA) (Q500, TA Instruments). TGA was performed under a nitrogen atmosphere at a ramping rate of 10 °C/min from 20 to 600 °C. The self-suspended hairy nanoparticles used to create the oligomer suspensions used in the study were found to have an inorganic content of 32.5 wt %, which translates to a core volume fraction of approximately 0.23. The inorganic content of the hairy nanoparticle suspensions was determined to be 24.7, 19.5, 10.0, and 3.8 wt %, which translates to core volume fractions ranging from 0.17, 0.13, 0.065, and 0.024, respectively.

Thermal transitions of the PEG-tethered silica nanoparticles and their suspensions were accessed by differential scanning calorimetry (DSC) (Q2000, TA Instruments) at a fixed ramp rate of 10 °C/min under nitrogen flow. The materials were first heated to 100 °C to eliminate any thermal history, then cooled to −90 °C, and heated back to 100 °C. Measurements during the second heating cycle were used to obtain the melting temperature, recrystallization temperature, and crystallinity. As shown in Figure 2, the melting and recrystallization temperatures of the self-suspended nanoparticles (ϕ_c = 0.23) are lower than those of untethered mPEG-OH. This result has been reported in the previous literature and attributed to tethering and confinement of the polymer by associated nanoparticles.[33,35] For hairy nanoparticles diluted with mPEGm, the $T_{m,1}$ and $T_{c,1}$ that are associated with the mPEG-OH (5k Da) decrease as the extent of dilution increases.

The $T_{m,2}$ and $T_{c,2}$ values that are associated with the oligomer mPEGm (500 Da) are elevated in the hairy nanoparticle suspensions. Such thermal behavior has been observed for miscible polymer blends and suggests that the tethered PEG chains and the oligomer solvent interact substantially and likely co-crystallize to some extent.[36] The crystallinity associated with the 5k Da PEG chains is observed to decrease, while that associated with the 500 Da oligomer solvent increases as the extent of dilution increases, which is expected with the change in the relative composition of tethered PEG and oligomer solvent. Noticeably, a third minor melting peak is observed at a temperature between the melting transitions of the neat mPEG-OH (5k Da) and mPEGm (500 Da) when the hairy nanoparticles are sufficiently diluted with the oligomer solvent. We tentatively attribute this observation to co-crystallization of the tethered PEG and the untethered oligomer.

Small-Angle X-Ray Scattering (SAXS). SAXS measurements were conducted using a SAXSess (Anton Paar) bench-top X-ray scattering system. The instrument utilizes a line collimated beam at a wavelength of 0.1542 nm with a block camera setup for data collection. The hairy nanoparticle suspensions were measured at 90 °C, which is above the melting temperature of the materials. The experimental, line collimated intensity, $I_{exp}(q)$, is related to the point collimated intensity, $I_0(q)$, by[37,38]

https://dx.doi.org/10.1021/acs.macromol.0c01448
Macromolecules 2021, 54, 426−439

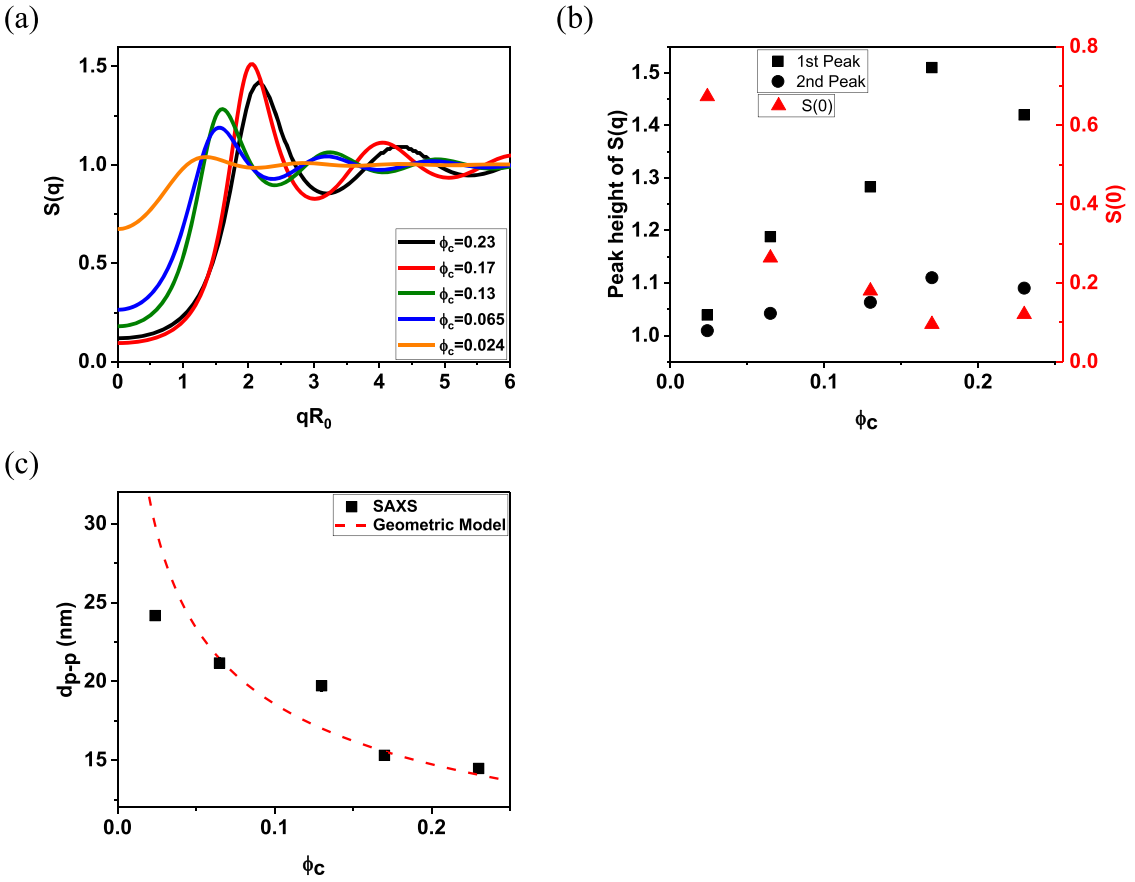

Figure 3. (a) Structure factor $S(q)$ of hairy nanoparticle suspensions in various dilutions at 90 °C as a function of normalized wave vector qR_0. (b) First and second peak heights of $S(q)$, and $S(q)$ at zero wave vector, of hairy nanoparticle suspensions in various dilutions as a function of the core volume fraction. (c) Average interparticle distance estimated from SAXS and a simple geometric model assuming random close packing as a function of the core volume fraction (for calculation see Section 2 in the Supporting Information). R_0 is the average radius of the nanoparticle cores and $R_0 \approx 5$ nm.

$$I_{exp}(q) = \int_{-\infty}^{\infty}\int_{-\infty}^{\infty} W_x(x)W_y(y)I_0\left(\sqrt{\left(\frac{\lambda aq}{2\pi} - y\right)^2 + x^2}\right)$$

where $W_x(x)$ and $W_y(y)$ are the horizontal and vertical X-ray beam profiles, respectively, q is the scattering wave vector, a is the sample-to-detector distance, and x and y are the horizontal and vertical dimensions, respectively. The generalized indirect Fourier transformation (GIFT) method was adopted to desmear the $I_{exp}(q)$ data to obtain $I_0(q)$. The scattering intensity of the particles, $I_{particle}$, can be written as[39]

$$I_{particle} = I_{particle/medium} - \phi_{medium} I_{medium}$$

where $I_{particle/medium}$ is the scattering intensity of the particles in a suspending medium, I_{medium} is the scattering intensity of the suspending medium, and ϕ_{medium} is the volume fraction of the suspending medium. It is known that for a suspension of spherical particles[27,38]

$$I_{particle}(q) = \phi_c \Delta\rho_e^2 VP(q)S(q)$$

where ϕ_c is the core volume fraction, $\Delta\rho_e$ is the electron density contrast, V is the volume of a single particle, $P(q)$ is the form factor, and $S(q)$ is the structure factor. In the dilute limit of particle concentration, the interparticle correlations vanish, and $S(q) \rightarrow 1$, such that the form factor $P(q)$ can be directly obtained from the scattering intensity. A diluted aqueous suspension of bare charge-stabilized silica nanoparticles (LUDOX SM30) was measured by SAXS for this purpose. The structure factor was then obtained by the GIFT method via a hard sphere structure factor model using the Percus−Yevick closure relation.

Rheology. All rheology measurements were performed at 90 °C, which is above the melting temperature of PEG. Dynamic oscillatory shear rheology and creep experiments were conducted using a stress-controlled MCR 501 (Anton Paar) mechanical rheometer outfitted with a cone and plate geometry (10 mm diameter, 2° cone angle). Materials used in the studies were rigorously dried under high vacuum overnight before being loaded into the rheometer. Samples were protected during the measurements using a dry nitrogen blanket. A previously established oscillatory time sweep protocol with an ultrasmall amplitude of $\gamma = 0.01\%$ and an angular frequency of $\omega = 1$ rad/s was used to monitor the evolution of the material properties with time.[33] The time sweep measurements were complemented with large amplitude oscillatory shear (LAOS) analysis at a fixed angular frequency $\omega = 1$ rad/s with shear strain γ ranging from 0.01 to 200%. Previous studies have found that the storage modulus G' and loss modulus G'' in LAOS measurements of self-suspended hairy nanoparticles exhibit plateau values at low strains. As the shear strain increases, the plateau regime is followed by a decay in G', which is associated with strain softening of the materials, and the emergence of a distinct G'' maximum, which is attributed to the yielding of the materials from cage breakup.[26,27,29,33,40] Such rationale is hereby used to understand the behavior of hairy nanoparticle suspensions. The caging dynamics were further probed by an established protocol of creep and recovery experiments,[33] where the materials that were deemed equilibrated on the basis of the time sweep analysis were first presheared in LAOS at a fixed angular frequency $\omega = 1$ rad/s and shear strain $\gamma = 100\%$ for 200 s and then interrogated by imposition of a step stress σ for 1800 s, followed by removal of the stress for another

https://dx.doi.org/10.1021/acs.macromol.0c01448
Macromolecules 2021, 54, 426−439

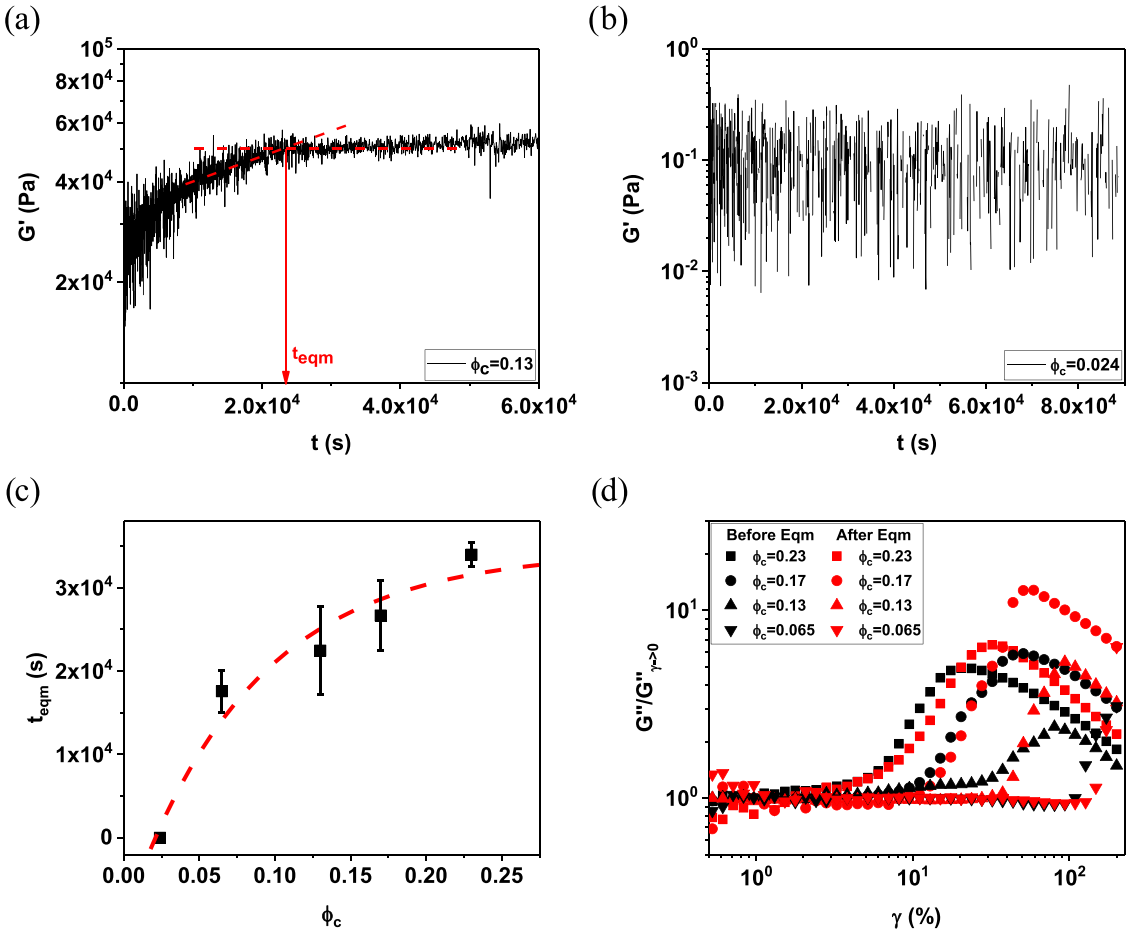

Figure 4. Small amplitude oscillatory time sweep of the unannealed hairy nanoparticle suspensions: (a) within the soft glassy regime (ϕ_c = 0.13) and (b) outside of the soft glassy regime (ϕ_c = 0.024). The time sweep is done at γ = 0.01% and ω = 1 rad/s at 90 °C. (c) Equilibration time of hairy nanoparticle suspensions as a function of the core volume fraction. An exponential fit of $t_{eqm} \cong -4.4 \times 10^4 \exp\left(-\frac{\phi_c}{0.08}\right) + 34000$ is shown in the dashed line. (d) Normalized loss modulus in large amplitude oscillatory strain sweep of the hairy nanoparticle suspensions before and after equilibration as a function of strain.

1800 s. The strain response recorded is reported relative to any residual strain present in the materials at time zero after imposition of the step stress.

To understand the stress contributions constituting the caging of the materials, we employed two rheological protocols: a shear reversal[34] and a shear-rest-shear-reverse using a strain-controlled ARES-LS (Rheometric Scientific) rheometer outfitted with a cone and plate geometry (10 mm diameter, 4° cone angle) on the materials deemed equilibrated based on results from transient experiments. Before each of the measurements, a preshear using the shear reversal protocol at 0.01 s^{-1} was performed. The stress response recorded is reported relative to the average of steady state stress in the forward and reversed shearing.

Spectroscopic Analysis. The conformation states of polymer chains in self-suspended hairy nanoparticles and their oligomer suspensions were characterized at 298 K by attenuated total reflectance Fourier-transform infrared spectroscopy (ATR FT-IR) (Thermal Fischer Scientific, Nicolet iS10). Two pairs of absorbance bands corresponding to the trans vs gauche conformations of C−O (1241 cm^{-1} vs 1280 cm^{-1}) and C−C (1342 cm^{-1} vs 1360 cm^{-1}) bonds were identified for the materials.[35] For the neat oligomer solvent mPEGm, the IR absorbance associated with the trans vs gauche conformations was identified to be 1248 cm^{-1} vs 1294 cm^{-1} for C−O and 1324 cm^{-1} vs 1349 cm^{-1} for C−C.[41,42]

The effects of crowding and confinement on the conformation states of the tethered chains were also characterized by Raman spectroscopy (Renishaw inVia) at 298 K. These measurements were performed using the self-suspended hairy nanoparticles, untethered neat mPEG-OH, and SiO_2-PEG/mPEGm suspensions. A fixed excitation wavelength of 785 nm was used for all studies to minimize contamination of the Raman scattering from the fluorescence background signal from impurities in the materials. Raman scattering at 797 and 860 cm^{-1} was conclusively identified to vibration modes associated with the trans−trans−trans (ttt) and trans−gauche−trans (tgt) conformations of ($-CH_2-CH_2-O$), respectively.[43]

RESULTS AND DISCUSSION

Structural Characteristics. Figure 3a reports the structure factor $S(q)$ of the self-suspended SiO_2-PEG particles and the SiO_2-PEG/mPEGm suspensions used in the study. The results show appreciable changes in $S(q)$ as the hairy nanoparticles are diluted with the oligomer solvent. Based on previous combined experimental and density functional theoretical studies,[44,45] the $S(q)$ maximum/peak apparent at the lowest q values is thought to reflect the repulsive interactions between the hairy nanoparticles. The second peak in $S(q)$ observed at higher q arises from the entropic attractions between the tethered polymer corona due to the space-filling constraint. As the extent of dilution increases, both the first and second peaks of $S(q)$ initially rise and then decay (see Figure 3b). This observation is counter-intuitive to the general expectation that dilution of a homogeneous particle suspension leads to larger

https://dx.doi.org/10.1021/acs.macromol.0c01448
Macromolecules 2021, 54, 426−439

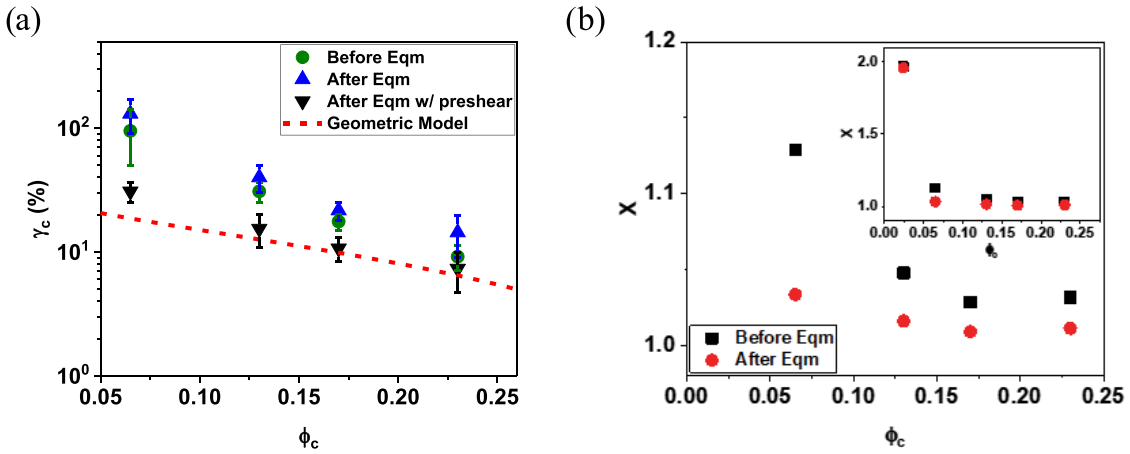

Figure 5. (a) Yield strain of hairy nanoparticle suspensions before equilibration, after equilibration, and after equilibration with a preshear, as a function of the core volume fraction, in comparison with a previously proposed geometric model. The preshear protocol is the same as the LAOS measurement. (b) Noise temperature, X, of the hairy nanoparticle suspensions within the soft glassy regime before and after equilibration as a function of the core volume fraction. The inset is the X vs core volume fraction with the hairy nanoparticle system outside the soft glassy regime included.

interparticle distances and less correlated cores. Dilution would also be expected to weaken the space-filling constraint on corona chains in the self-suspended SiO_2-PEG system, systematically reducing the size of the second $S(q)$ maximum with dilution. Our observations are nonetheless consistent with an earlier report in which this so-called structural anomaly was reported in suspensions of silica nanoparticles ionically grafted with PEG oligomers dispersed in untethered PEG oligomers.[46] According to the authors, the anomaly likely arises from the softness of the molecular repulsion between the hairy nanoparticles, such that the initial addition of the oligomer solvents leads to a strong entropic gain that overcompensates the energetic cost of molecular overlap, producing more enhanced interparticle correlations.

Figure 3b (right) reports the structure factor values estimated in the limit of zero wave vector $S(0)$ as a function of ϕ_c. $S(0)$ is observed to first decrease moderately and then increase strongly as the hairy nanoparticles are diluted with the oligomer. It is known from the literature that $S(0)$ is related to the isothermal compressibility and as such is a reflection of the magnitude of long-wavelength density fluctuations in the materials.[37,47] Figure 3b therefore suggests that the long-wavelength density fluctuation in our hairy nanoparticle systems is initially more suppressed upon dilution but ultimately grows substantially as the SiO_2 nanoparticle cores are pushed further apart by PEG oligomer molecules. Previous theoretical work has shown that polydispersity in both the nanoparticle core size and grafting density can lead to an elevation in $S(0)$, with polydispersity in grafting density having the larger effect.[44] The observation has been explained in terms of the effect of each hairy particle in the polydisperse systems carrying different amounts of the tethered polymer as solvent.[44] On this basis, we suspect that the $S(0)$ anomaly arises from the fact that the initial addition of the oligomer solvent saturates the effect of polydispersity of the tethered corona and makes the particles more uniformly distributed, leading to a decrease in the long-wavelength density fluctuations. As the materials are further diluted, the effects of relieving geometric confinement and softening of the tethered chain interactions lead to weaker suppression of the long-wavelength density fluctuations and thus result in higher $S(0)$. It is known that the position of the first peak in $S(q)$, q_1, is related to the average interparticle distance, d_{p-p}, of the hairy nanoparticles by $d_{p-p} = 2\pi/q_1$. Figure 3c shows the d_{p-p} obtained from the SAXS results and from estimation of random close packing of the particles, where the results agree reasonably well.

Rheological Behavior. Recently, we reported that self-suspended hairy nanoparticles undergo a significant equilibration process that reflects the slow development of the equilibrium cage structure in the materials. The process is readily seen in transient ultrasmall amplitude oscillatory shear rheology experiments as a gradual rise of the elastic modulus with time.[33] The same methodology was applied to the hairy nanoparticle suspensions to investigate the effect of ϕ_c on the equilibration process. Results reported in Figure 4a and in the Supporting Information show that like the self-suspended systems, the SiO_2-PEG/mPEGm suspensions also manifest the slow equilibration behavior, wherein the storage modulus G' increases slowly but substantially toward a plateau value. The behavior persists for $\phi_c > \phi^* \approx 0.024$, when it appears that the separation between the nanoparticle cores becomes large enough for the materials transit out of the soft glassy state, resulting in an essentially instantaneous equilibration (Figure 4b).

The equilibration time, t_{eqm}, can be estimated from $G'(t)$ data as shown in Figure 4a and the results are reported in Figure 4c. It is seen that t_{eqm} decreases as the extent of dilution increases according to the approximate relation $t_{eqm} \cong -4.4 \times 10^4 \exp\left(-\frac{\phi_c}{0.08}\right) + 34000$. The acceleration of equilibration is expected. It likely originates from the faster configurational dynamics of the materials due to the addition of the low-molecular-weight oligomer solvent. We note nonetheless that before transiting out of the glassy state, the acceleration in equilibration appears to be much weaker compared to the nearly 3 orders of magnitude drop in G' as the materials are diluted. We suspect that the behavior reflects the counterbalancing influences of the oligomer addition, where the acceleration of chain dynamics tends to reduce t_{eqm} and the relief in geometric confinement mitigates the driving force for the equilibration.

https://dx.doi.org/10.1021/acs.macromol.0c01448
Macromolecules 2021, 54, 426−439

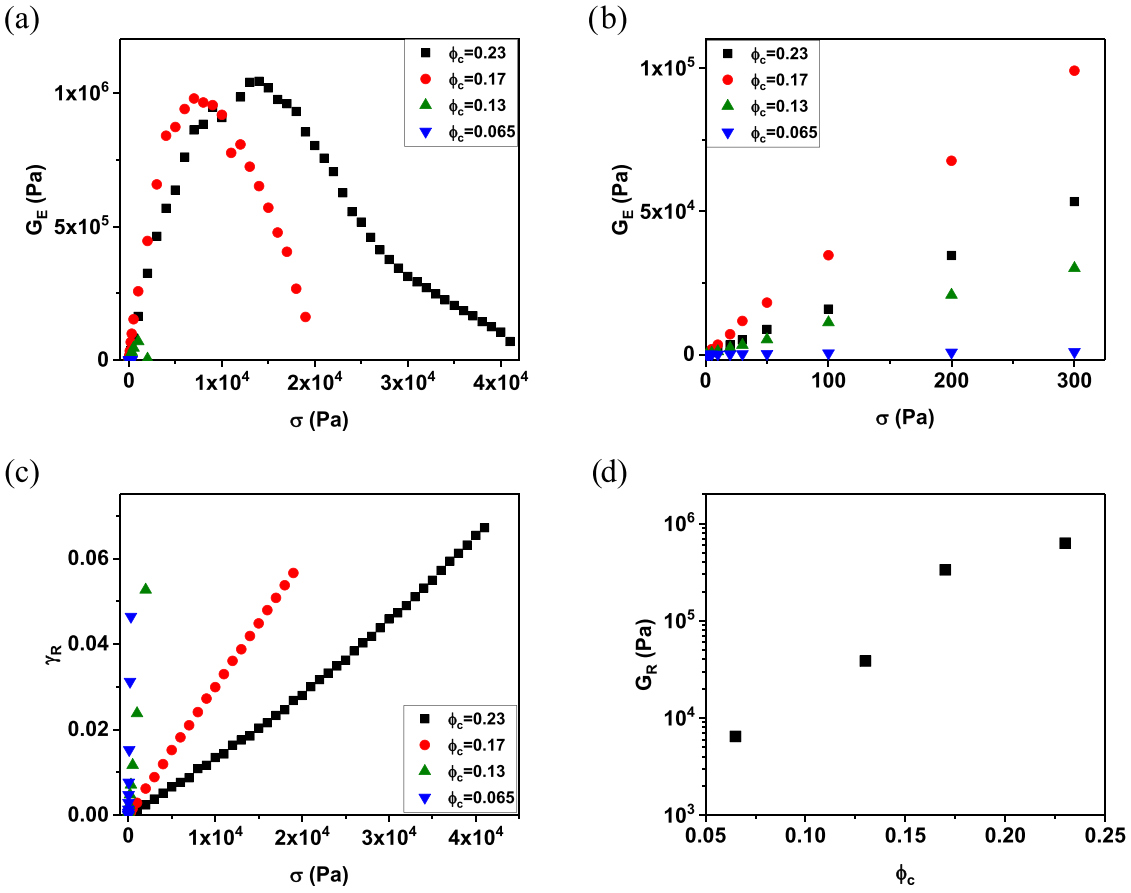

Figure 6. (a) Effective modulus (G_E) of hairy nanoparticle suspensions as a function of stress (σ) applied in creep. (b) G_E as a function of σ of hairy nanoparticle suspensions within the soft glassy regime shows a linear relationship at low stress. (c) γ_R as a function of σ of hairy nanoparticle suspensions shows a linear relationship. (d) G_R of the hairy nanoparticle suspensions as a function of the core volume fraction.

Figure 4d reports normalized strain-dependent loss moduli G'' (γ) measured using large amplitude oscillatory shear (LAOS) measurements at fixed oscillation frequency, before and after the equilibration process. It is known from the literature that the G'' maximum observed at modest shear strains is associated with the cage breakup or yielding of soft glassy materials.[23,24] For the hairy nanoparticle suspensions with $\phi_c > \phi_c^*$, the G'' maximum is enhanced and shifts to higher strain as the materials are equilibrated. Similar behavior has been previously reported for self-suspended hairy nanoparticles and was attributed to the strengthening of caging by enhanced chain interpenetration and entanglements. The shift of the G'' maximum to higher shear strains as the core volume fraction of the materials decreases has also been previously observed for self-suspended hairy nanoparticles and was attributed to an increase in the relative uninterpenetrated length of the tethered chains, which allows the material elements to move on a larger length scale before the cage itself begins to be deformed and ultimately break down.[33] The value of the shear strain at cage breakdown, i.e. the yield strain γ_c, can be estimated by $\gamma_c = a_u/d_{p-p}$, where a_u is the uninterpenetrated length and d_{p-p} is the average interparticle distance. After simplification [see Section 4 in the Supporting Information], γ_c can be shown to depend solely on the core volume fraction ϕ_c by $\gamma_c = 0.42 - 0.58\phi_c^{1/3}$. It is then apparent that $\gamma_c \to 0$ when $\phi_c \to 0.38$, at which point the particles can be thought of as fully interlocked by interpenetrating chains and are thus unable to move without deforming the cage. This result is also consistent with literature reports, which show that the viscosity of self-suspended hairy nanoparticles diverges at $\phi_c \approx 0.25$, i.e., much smaller than the random close pack limit.[32] Figure 5a reports the experimental yield strain obtained from the LAOS analysis of the hairy nanoparticle suspensions at various stages in comparison with the yield strain predicted using the expression above. The fact that γ_c before equilibration appears higher than the model prediction likely arises from the less interpenetrated unequilibrated chain conformations, which leads to a higher a_u. The higher γ_c directly after equilibration may likewise arise from the extra strengthening effect due to chain entanglements.

The agreement between the predicted and measured γ_c values after equilibration indicates that the physics captured in the simple geometric model accurately captures the yielding transition in hairy particle suspensions with $\phi_c > \phi_c^*$. That the same model also accurately predicts γ_c self-suspended systems from a variety of sources[25,27−29,31,40,48] further confirms that it captures the right set of physics to describe yielding in these materials. Additionally, the finding means that the underlying physics of yielding and caging of all jammed hairy nanoparticle systems is likely the same—caging arises from chain interpenetration between adjacent particles driven by space-filling constraint, yielding results when the interpenetrated chains are deformed enough to break their associations. It follows that the process is entirely reversible, which is also in accord with the experiment.[25−27,29,31,33,40] The potential deviation of the model prediction and the experimental results at low ϕ_c likely

https://dx.doi.org/10.1021/acs.macromol.0c01448
Macromolecules 2021, 54, 426−439

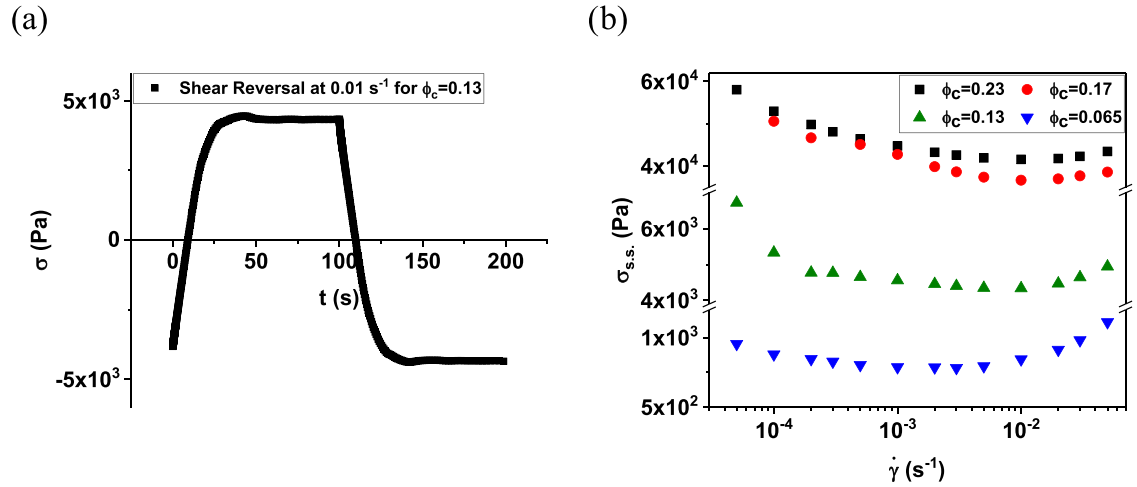

Figure 7. (a) Illustration of the shear reversal protocol on equilibrated hairy nanoparticle suspensions, where the materials are subjected to a forward specified shear $\dot{\gamma}_i$ to steady state, followed by a sudden reverse in shear direction to steady state. The measurements are done at 90 °C. (b) Steady state shear stress as a function of the shear rate of hairy nanoparticle suspensions in various dilutions.

arises from the oversimplification of the model, in which the uninterpenetrated section is treated as a string but in reality is more likely a coil. Therefore, to induce a certain stress, a higher strain is needed, and such effect is more significant at low ϕ_c.

In soft glassy materials, the noise temperature $X = 1 + 2\delta/\pi$ is thought to provide a more useful variable than the thermodynamic temperature T for measuring the driving force for structural relaxation. Figure 5b reports X for the SiO_2/mPEGm system as a function of ϕ_c. The results were obtained from tan δ measurements in the linear viscoelastic regime, before and after equilibration. It is apparent that the driving force for structural relaxation is reduced upon equilibration, which is consistent with our previous argument that during the equilibration process, tethered chains adopt more interpenetrated conformations, which enhances caging.[33] The noise temperature also increases as the extent of dilution increases, which likely originates from the weakening of the cages due to addition of oligomer solvent. Moreover, it is evident that X remains low as the hairy nanoparticles are diluted until the critical core volume fraction, ϕ^*, is reached, whence X increases dramatically and the materials unjam.

A methodology of creep and recovery was previously established to directly probe into cage dynamics, in which the materials were first presheared above the yield strain to destroy the existing cages, then subjected to a specified shear stress σ, followed by the removal of applied stress.[33] When the specified stress is below a certain value, the creep of the materials will be self-arrested and the strain plateaus. From the plateau strain γ_p, an effective modulus G_E can be defined as $G_E = \sigma/\gamma_p$. Upon stress removal, a portion of the strain will be instantly recovered, which we denote as γ_R, from which a recovery modulus G_R can be defined as $G_R = \sigma/\gamma_R$. Figure 6a reports the G_E of the hairy nanoparticle systems that still reside in the soft glassy regime. The G_E exhibits a maximum with applied σ and both the G_E maximum and the σ where this maximum occurs shift to lower values as the extent of dilution increases. The exhibition of a maximum in G_E has been observed in the self-suspended hairy nanoparticles,[33] and the results in Figure 6a are consistent with the expectation that the addition of oligomer solvents weakens the cages and thus lowers the maximum effective strength of the reformed cage and the highest stress the materials can sustain without flowing continuously in the creep process. More importantly, a linear dependence of G_E on σ at low stress that was observed in self-suspended hairy nanoparticles[33] is also observed for the hairy nanoparticle suspensions, as illustrated in Figure 6b. The results suggest that when the applied σ is low, the creep of the materials is essentially self-arrested at the same strain irrespective of the applied σ, which implies distinct subcage and cage regimes even for hairy nanoparticle suspensions that are substantially diluted. The recovered strain γ_R with respect to applied σ is shown in Figure 6c, where G_R can be obtained from the inverse slope and is reported in Figure 6d. The G_R is observed to decrease as the extent of dilution increases, which is expected due to the softening effect of the oligomer solvent. The fact that γ_R is linear with σ suggests that the cage essentially maintains its elasticity as long as the materials can self-arrest during the creep, irrespective of the γ_p where the deformation stops. Such linearity has been previously observed for self-suspended hairy nanoparticles,[33] and the current results suggest that before transiting out of the soft glassy regime, the oligomer suspensions of hairy nanoparticles essentially retain the caging dynamics of the hairy nanoparticles.

While the material responses of the oligomer suspensions of hairy nanoparticles are governed by the same underlying physics of the self-suspended hairy nanoparticles, it is noticed that the G' of the suspensions is considerably lower than that of the self-suspended materials at the same ϕ_c, as illustrated in Figure S5. Such a decrease in modulus is expected to come from the untethered nature of the oligomer solvent, where it relaxes in a free manner in contrast to the tethered chains. Moreover, the infrared results (Figure 9c,d) show that the added oligomers in the hairy nanoparticle suspensions no longer exhibit the characteristic frequencies of the neat oligomers but rather display frequencies of the tethered chains. It suggests that the tethered chains of the hairy nanoparticles potentially have a coupling effect, such that the added oligomers no longer exist in their original configurations.

In an attempt to understand molecularly the origins of caging in the hairy nanoparticle systems, we were inspired by a recent study by Lin et al. using a specially designed methodology of shear reversal to analyze the contributions of hydrodynamics and contact in the overall stress response of shear thickening colloidal suspensions.[34] In the experiment, the

https://dx.doi.org/10.1021/acs.macromol.0c01448
Macromolecules 2021, 54, 426−439

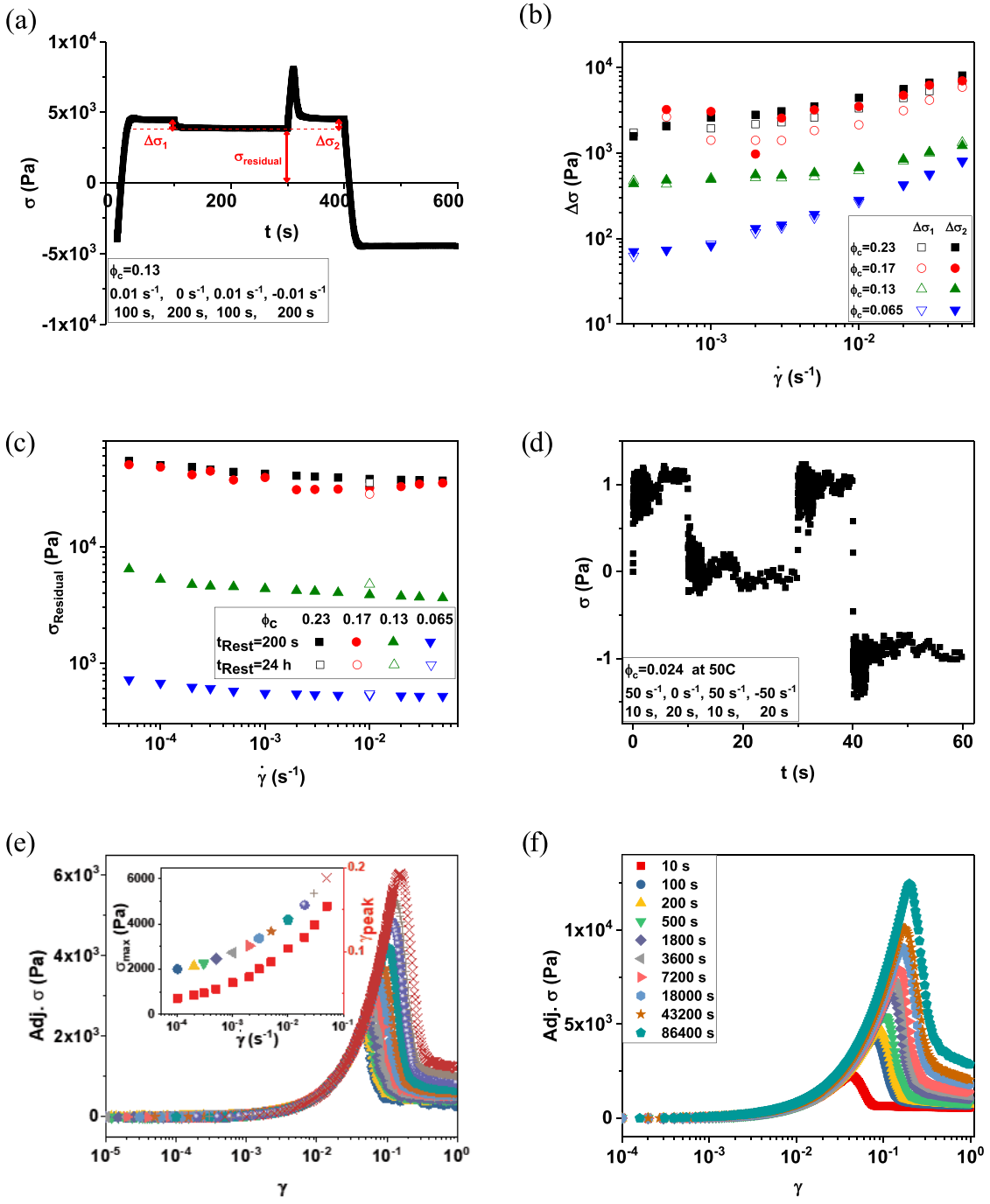

Figure 8. (a) Illustration of shear-rest-shear-reverse on equilibrated hairy nanoparticle suspensions, where the materials are subjected to a forward specified shear ($\dot{\gamma}_i$) to steady state, followed by a rest stage of a specified time (200 s, unless otherwise mentioned), and reinitiated to flow at $\dot{\gamma}_i$ to steady state, followed by a sudden reverse in shear direction. The measurements are performed at 90 °C. (b) Stress difference between steady state stress under shearing and residual stress after flow cessation as a function of the shear rate for hairy nanoparticle suspensions. (c) Residual stress of hairy nanoparticle suspensions as a function of the shear rate before flow cessation. (d) Shear-rest-shear-reverse results of hairy nanoparticle suspension out of the soft glassy regime. (e) Stress overshoot of a hairy nanoparticle suspension (ϕ_c = 0.13) upon flow reinitiation at varied shear rates with a rest time of 200 s as a function of cumulative strain. The inset shows the maximum stress in the overshoot (left axis) as a function of the shear rate, which also serves as the legend, and the strain associated with the stress maximum (right axis). (f) Stress overshoot of a hairy nanoparticle suspension (ϕ_c = 0.13) upon flow reinitiation with varied rest time at a shear rate of 0.01 s^{-1}, as a function of cumulative strain.

materials were first sheared to steady state, followed by a sudden reverse in shear direction. The idea is that, upon the reversal in shear, the hydrodynamic stress remains but in an opposite direction, whereas the contact stress instantaneously drops to zero and needs time to develop. We adopt the same shear reversal methodology to examine the hairy nanoparticle suspensions, where a representative result of the hairy nanoparticle suspensions in the soft glassy regime is shown in Figure 7a. What appears immediate to us is the observation that the stress does not drop to zero or a finite negative value upon reversal in shear direction, as would be expected for the vanished contact stress and remaining hydrodynamic stress,

https://dx.doi.org/10.1021/acs.macromol.0c01448
Macromolecules 2021, 54, 426−439

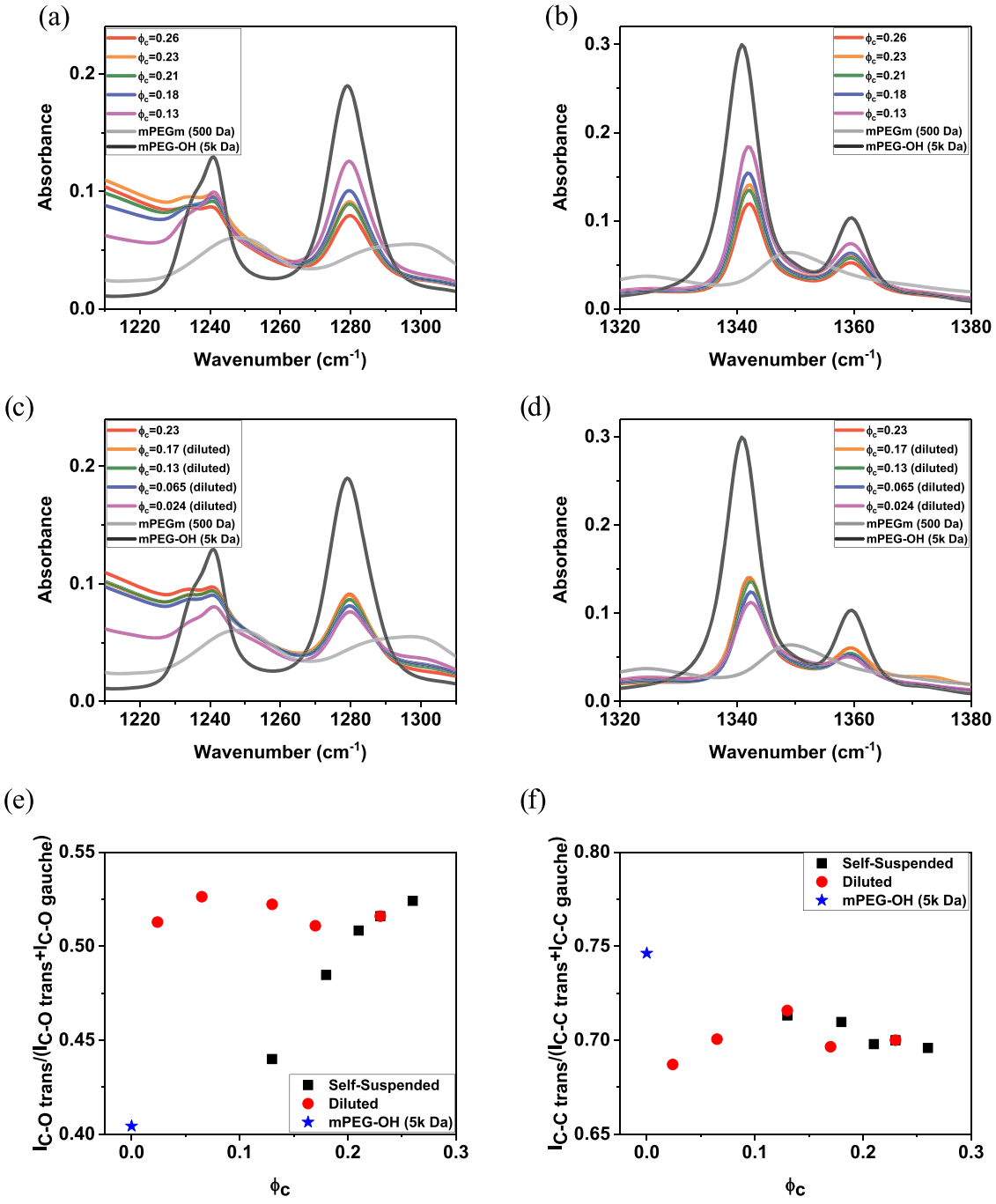

Figure 9. IR absorbance associated with the C−O trans vs gauche (1241 cm^{-1} vs 1280 cm^{-1}) and C−C trans vs gauche (1342 cm^{-1} vs 1360 cm^{-1}) of (a, b) self-suspended hairy nanoparticles and (c, d) hairy nanoparticle suspensions in comparison with untethered PEG and oligomer solvent. Relative absorbance of trans conformation for (e) C−O and (f) C−C bonds of self-suspended hairy nanoparticles and hairy nanoparticle suspensions as a function of the core volume fraction.

but rather changes slowly toward the new steady state. From the steady state stress $\sigma_{s.s.}$ at each specified shear rate $\dot{\gamma}$, the flow curves of the materials can be obtained.

As shown in Figure 7b, the flow curves of the hairy nanoparticle suspensions exhibit a peculiar pattern, where an upturn in stress is observed at low $\dot{\gamma}$. Such flow curves are substantially different from those of typical colloidal soft glassy materials that follow the Herschel−Bulkley equation $\sigma = \sigma_y + \eta\dot{\gamma}^n$ where σ_y, η, and n are the yield stress, effective viscosity, and a scaling exponent, respectively, in which a plateau corresponding to yield stress would be observed at low $\dot{\gamma}$.[49] They are also considerably different from the flow curves of star polymer glasses, in which case the stress will further decay when the time scale associated with the shear rate becomes longer than the longest relaxation time of the star arms.[50] To the best of our knowledge, such peculiar flow curves are observed for the first time in soft glassy materials, and we attribute the upturn at low $\dot{\gamma}$ to the simultaneous reengagement of tethered chains during deformation, such that when the shear rate is slow enough, more molecular friction is imposed to the flow, leading to an elevation in shear stress.

https://dx.doi.org/10.1021/acs.macromol.0c01448
Macromolecules 2021, 54, 426−439

To desmear the stress contributions in the materials, we further developed a protocol of shear-rest-shear-reverse. As illustrated in Figure 8a, the materials are first sheared to steady state in the forward direction, followed by a rest stage, and then sheared again in the forward direction, followed by a reversal in the shearing direction. A drop in stress $\Delta\sigma_1$ is observed when the flow is stopped, and a significant unrelaxable stress $\sigma_{residual}$ is found in the rest stage. Upon flow reinitiation, the stress exhibits an overshoot before reaching a plateau, where the difference between the plateau stress and $\sigma_{residual}$ is denoted as $\Delta\sigma_2$. As reported in Figure 8b, the $\Delta\sigma_1$ and $\Delta\sigma_2$ both relate to the difference between steady state stress under flow and the residual stress under rest and match with each other closely. It implies that such stress difference likely originates from the flow of the materials and can be regarded as a dynamic friction in the materials under motion. The stress differences also increase with $\dot{\gamma}$ and the behavior more closely resembles the Herschel−Bulkley equation, or in other words, the typical flow curves of colloidal glasses.

As shown in Figure 8c, the residual stress $\sigma_{residual}$ exhibits a mild upturn at low $\dot{\gamma}$, which likely accounts for the upturn in the overall flow curves earlier mentioned. In addition, the $\gamma_{residual}$ is observed to be preserved even with a rest time of 24 h at a temperature nearly 140 °C above the glass transition temperature of the tethered chains for the substantially diluted hairy nanoparticle suspension ($\phi_c = 0.065$), which implies that the $\gamma_{residual}$ of the materials might never relax by themselves. Such observation is in accordance with the potential energy landscape proposed in the SGR model on the explanation of caging, in which the thermal energy alone is far from enough to match up the potential energy depth to allow the material elements to escape the cages.[24] The residual stress has also been observed in the literature for two polymer-tethered surfaces under compression and was attributed to the chain orientations that do not relax under the measurement time scale.[51] As their systems bear a close analogy with our hairy nanoparticle systems where tethered chains are confined between geometric surfaces, it implies that the $\gamma_{residual}$ likely originates from the orientation of the interpenetrated chains and can be regarded as some static friction that the materials have to overcome before they can start flowing. When the extent of dilution is high enough such that the materials transit out of the soft glassy regime, the caging behavior is lost and the $\gamma_{residual}$ no longer exists, as illustrated in Figure 8d. The stress overshoot upon flow reinitiation at different $\dot{\gamma}$ is shown in Figure 8e, where the maximum stress and the cumulative strain that the maximum stress resides both increase as $\dot{\gamma}$ increases. Such stress overshoot has been previously observed in shear startup of the hairy nanoparticle systems as well as generic soft glassy materials and is believed to reflect the yielding or cage breakup in the materials.[27,40] In the framework of a previously proposed geometric model, the interpenetrated sections of tethered chains form the cages such that the material elements can only move on the length scale of uninterpenetrated sections without disturbing the cages.[33] When subjected to flow, a faster pulling on the "rigid" cages reasonably induces a higher stress before it destroys the cages. Figure 8f illustrates the effects of rest time on the stress overshoot in flow reinitiation. Both the stress maximum and the cumulative strain associated increase with rest time. The observation is consistent with the geometric model framework that shows that the reengagement of interpenetrated chains for longer time leads to strengthened cages whose impairment require higher stress and larger deformation, as well as the LAOS analysis that indicates the shift of yield strain to a higher value upon equilibration.

It should be noted that the peculiar upturn of the flow curve in Figure 7b is suggestive of shear banding in thixotropic soft glassy materials.[52] Below a sufficient shear rate, the structure in the materials cannot be fully destroyed, such that the materials undergo nonaffine deformation, e.g., shear bands of the critical shear rate and zero shear rate.[53] Beyond some critical shear rate, the structure in the materials can be eliminated by the deformation and the material behavior follows back to the Herschel−Bulkley equation.

Spectroscopic Analysis. To verify our molecular explanation of caging in hairy nanoparticle systems, we employed infrared (IR) and Raman spectroscopy to access the effects of geometric confinement on polymer chain conformations. We identified two conformation pairs in IR spectra that correspond to C−O trans vs gauche (1241 cm^{-1} vs 1280 cm^{-1}) and C−C trans vs gauche (1342 cm^{-1} vs 1360 cm^{-1}) of PEG.[35] The absorbance of the conformations is reported in Figure 9a−d for the self-suspended hairy nanoparticles and the hairy nanoparticle suspensions.

The absorbance of the vibration modes $A(\nu)$ is known to follow the Bouger−Lambert−Beer law, $A(\nu) = \sum[a_i(\nu)bc_i]$, where $a_i(\nu)$, b, c_i are the absorbance of component i, light path length, and concentration of componenet i, respectively.[54] It thus allows us to use the peak intensity to estimate the relative compositions of the conformation pairs. While the absorbance ratio of C−C conformations in the self-suspended hairy nanoparticles does not appear to vary much, an obvious change can be observed in C−O conformations as the core volume fraction varies. For the hairy nanoparticle suspensions, however, both the C−O and C−C conformations lack a direct trend with ϕ_c.

The relative intensity of the C−O and C−C conformations is reported in Figure 9e,f. For the self-suspended hairy nanoparticles, the relative fraction of C−O trans conformation increases substantially as ϕ_c increases. In the meantime, minimal variation is observed in the relative fraction of C−C trans conformation. Since ϕ_c reflects the extent of geometric confinement, the results suggest that the tethered chains in the self-suspended hairy nanoparticles likely adopt more *trans* conformations overall, which is consistent with the idea that geometric confinement leads to more extended and interpenetrated chains that induce caging. For the oligomer suspensions of hairy nanoparticles, the conformations of the tethered chains are obscured by the oligomer solvent. Due to the low molecular weight of 500 Da, the estimated radius of gyration of the oligomer is ∼0.8 nm, which just matches the Kuhn length of PEG (0.82 nm).[55] In other words, the oligomer is not long enough to observe the Gaussian coil conformation but might rather exhibit a preference in the molecular orientation, as evidenced in the trans vs gauche ratios that apparently differ from those of 5k Da PEG, as shown in Figure 9. Surprisingly, even for hairy nanoparticle suspensions that are diluted out of the soft glassy regime ($\phi_c = 0.024$), there are still no absorbance peaks of free oligomer solvent observed, implying that the vibrational modes of oligomer solvent now align with those of tethered chains. Such observation is consistent with the DSC analysis that suggests co-crystallization of the oligomer solvent and the tethered polymer.

https://dx.doi.org/10.1021/acs.macromol.0c01448
Macromolecules 2021, 54, 426−439

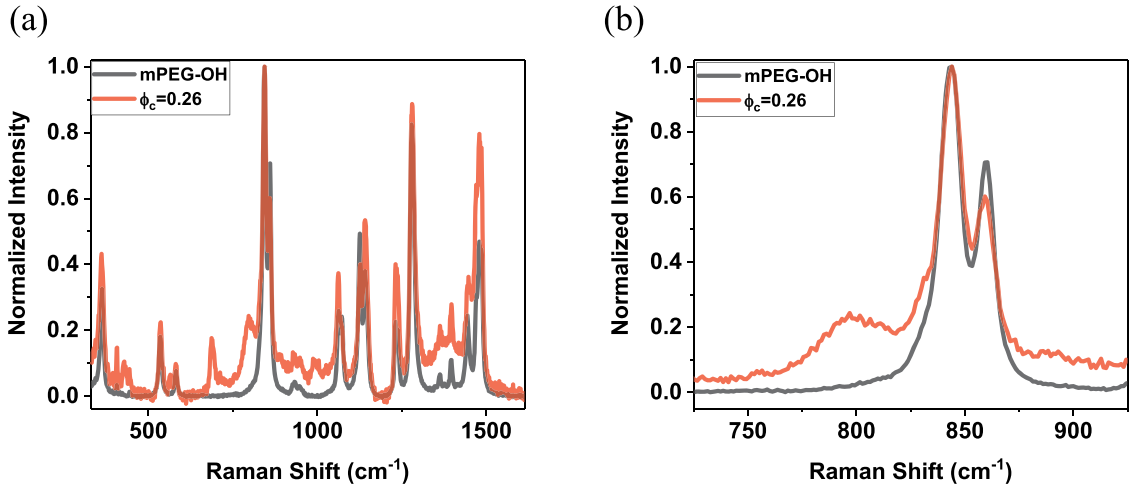

Figure 10. (a) Raman spectrum of self-suspended hairy nanoparticles in comparison with untethered PEG chains. (b) Zoom-in of the Raman spectrum where peaks at 797 and 860 cm^{-1} correspond to trans−trans−trans and trans−gauche−trans conformations of (−CH_2−CH_2−O), respectively.

The spectroscopic measurements were performed at room temperature due to experimental limitations and therefore cannot eliminate the complexation of material crystallinity. An underlying assumption is that a more interpenetrated system exhibits overall a higher fraction of trans conformations despite the material crystallinity.

For the oligomer suspensions, the ambient measurement temperature is above the melting temperature of the added oligomers, as illustrated in Figure 2b. Therefore, the oligomer solvent exists mostly in its amorphous form in the spectroscopic measurements. The potentially preferential orientations of the oligomer solvents compete with the effects of geometric confinement on tethered chain conformations in the infrared absorption, which leads to a complex pattern for the oligomer suspensions in the infrared spectra.

Figure 10 reports the Raman spectrum of a self-suspended hairy nanoparticle system in comparison with the untethered PEG. We can see that the tethering leads to several new peaks that are unique to the hairy nanoparticles. Among them, the peaks at 797 and 860 cm^{-1} are identified to correspond to the trans−trans−trans (ttt) and trans−gauche−trans (tgt) conformations of the PEG backbone unit (−CH_2−CH_2−O), respectively,[43] and are shown in Figure 10b. Compared to untethered PEG, the tethered PEG in hairy nanoparticles exhibits a boost in the peak of ttt and a reduction in the peak of tgt conformations. The results imply that the tethered chains under confinement overall adopt more trans conformations and are therefore likely in a more extended state. Such findings provide additional molecular evidence on the notion of enhanced chain interpenetration due to geometric confinement, which is believed to be the microscopic origins of caging in hairy nanoparticle systems.

CONCLUSIONS

We investigated the caging dynamics and structural evolution of PEG oligomer suspensions of model soft glassy materials composed of silica nanoparticles covalently tethered with PEG chains. The amount of oligomer addition modulates the extent of geometric confinement, which is reflected in the core volume fraction. The oligomer suspensions of hairy nanoparticles exhibit weakened primary and secondary structure factor peaks as the core volume fraction decreases, indicating that the nanoparticle cores are less correlated, and the corona chains are less interpenetrated as the geometric confinement relieves. LAOS and time sweep rheology measurements reveal that the hairy nanoparticle suspensions exhibit the typical caging behavior of solvent-free hairy nanoparticles up to a critical ϕ_c, where the materials transit out of the soft glassy regime. Creep and recovery experiments of hairy nanoparticle suspensions within the soft glassy regime indicate significant subcage motions similar to those of solvent-free hairy nanoparticles, implying that before a critical limit, even substantial addition of solvent would not change the caging dynamics in the hairy nanoparticle systems. The observation is consistent with the noise temperature obtained from the SGR model, where a sudden rise in noise temperature is coincided with the transition out of the soft glassy regime.

A peculiar flow curve with an upturn at low shear rates is observed for the first time for soft glassy materials, which is believed to originate from the extra resistance due to corona reengagement in the hairy nanoparticle soft glasses upon slow enough shear rates. Stress decomposition using a shear-rest-shear-reverse rheology protocol reveals a significant residual stress in the hairy nanoparticle soft glasses upon flow cessation, where the residual stress likely arises from the orientations of interpenetrated corona chains under confinement. Infrared and Raman spectroscopy suggests that the tethered chains adopt more extended conformations due to the geometric confinement, which provides molecular evidence on the enhanced chain interpenetration driven by geometric confinement. The overall caging behavior of hairy nanoparticle suspensions is in good accordance with the simple geometric model previously proposed for solvent-free hairy nanoparticles. As the hairy nanoparticle suspensions molecularly lie between colloidal glasses and star polymer glasses, the findings of the study would not only serve as good design principles for practical applications utilizing hairy nanoparticle derivatives but also help bridge the various subclasses of soft glassy materials.

ASSOCIATED CONTENT

Supporting Information

The Supporting Information is available free of charge at https://pubs.acs.org/doi/10.1021/acs.macromol.0c01448.

https://dx.doi.org/10.1021/acs.macromol.0c01448
Macromolecules 2021, 54, 426−439

Raw scattering intensities from SAXS measurements; calculation of d_{p-p}; ultrasmall amplitude oscillatory time sweep rheology; calculation of γ_c; comparison of equilibration of self-suspended and oligomer suspension of hairy nanoparticles; linear viscoelastic spectra (PDF)

AUTHOR INFORMATION

Corresponding Author

Lynden A. Archer − *Robert Frederick Smith School of Chemical and Biomolecular Engineering, Cornell University, Ithaca, New York 14853, United States;* orcid.org/0000-0001-9032-2772; Email: laa25@cornell.edu

Authors

Xiaotun Liu − *Robert Frederick Smith School of Chemical and Biomolecular Engineering, Cornell University, Ithaca, New York 14853, United States*

Nyalaliska W. Utomo − *Robert Frederick Smith School of Chemical and Biomolecular Engineering, Cornell University, Ithaca, New York 14853, United States*

Qing Zhao − *Robert Frederick Smith School of Chemical and Biomolecular Engineering, Cornell University, Ithaca, New York 14853, United States;* orcid.org/0000-0003-0625-9892

Jingxu Zheng − *Department of Materials Science and Engineering, Cornell University, Ithaca, New York 14853, United States*

Duhan Zhang − *Department of Mechanical and Aerospace Engineering, Cornell University, Ithaca, New York 14853, United States;* orcid.org/0000-0001-9428-956X

Complete contact information is available at: https://pubs.acs.org/10.1021/acs.macromol.0c01448

Notes

The authors declare no competing financial interest.

ACKNOWLEDGMENTS

This work was supported by the National Science Foundation, Award No. DMR-1609125. This work is based upon research conducted at the Cornell Energy Systems Institute (CESI). This work made use of the Cornell Center for Materials Research Shared Facilities, which are supported through the NSF MRSEC program (DMR-1719875).

REFERENCES

(1) Trappe, V.; Prasad, V.; Cipelletti, L.; Segre, P. N.; Weitz, D. A. Jamming phase diagram for attractive particles. *Nature* **2001**, *411*, 772−775.

(2) Cates, M. E.; Wittmer, J. P.; Bouchaud, J. P.; Claudin, P. Jamming, force chains, and fragile matter. *Phys. Rev. Lett.* **1998**, *81*, No. 1841.

(3) Srivastava, S.; Agarwal, P.; Archer, L. A. Tethered Nanoparticle-Polymer Composites: Phase Stability and Curvature. *Langmuir* **2012**, *28*, 6276−6281.

(4) Stiakakis, E.; Vlassopoulos, D.; Roovers, J. Thermal jamming in colloidal star-linear polymer mixtures. *Langmuir* **2003**, *19*, 6645−6649.

(5) Yang, J.; Schweizer, K. S. Tunable dynamic fragility and elasticity in dense suspensions of many-arm-star polymer colloids. *Europhys. Lett.* **2010**, *90*, No. 66001.

(6) Truzzolillo, D.; Vlassopoulos, D.; Gauthier, M. Osmotic Interactions, Rheology, and Arrested Phase Separation of Star−Linear Polymer Mixtures. *Macromolecules* **2011**, *44*, 5043−5052.

(7) Vlassopoulos, D. Colloidal star polymers: Models for studying dynamically arrested states in soft matter. *J. Polym. Sci., Part B: Polym. Phys.* **2004**, *42*, 2931−2941.

(8) Löwen, H.; Watzlawek, M.; Likos, C. N.; Schmidt, M.; Jusufi, A.; Denton, A. R. Phase transitions in colloidal suspensions and star polymer solutions. *J. Phys.: Condens. Matter* **2000**, *12*, No. A465.

(9) Helgeson, M. E.; Wagner, N. J.; Vlassopoulos, D. Viscoelasticity and shear melting of colloidal star polymer glasses. *J. Rheol.* **2007**, *51*, 297−316.

(10) Scheffold, F.; Cardinaux, F.; Mason, T. G. Linear and nonlinear rheology of dense emulsions across the glass and the jamming regimes. *J. Phys.: Condens. Matter* **2013**, *25*, No. 502101.

(11) Denkov, N. D.; Tcholakova, S.; Golemanov, K.; Lips, A. Jamming in Sheared Foams and Emulsions, Explained by Critical Instability of the Films between Neighboring Bubbles and Drops. *Phys. Rev. Lett.* **2009**, *103*, No. 118302.

(12) Zhang, H. P.; Makse, H. A. Jamming transition in emulsions and granular materials. *Phys. Rev. E* **2005**, *72*, No. 011301.

(13) Hattori, H. Anti-reflection surface with particle coating deposited by electrostatic attraction. *Adv. Mater.* **2001**, *13*, 51−54.

(14) Dąbroś, T.; Vandeven, T. G. M. Kinetics of Coating by Colloidal Particles. *J. Colloid Interface Sci.* **1982**, *89*, 232−244.

(15) Mihi, A.; Ocana, M.; Miguez, H. Oriented colloidal-crystal thin films by spin-coating microspheres dispersed in volatile media. *Adv. Mater.* **2006**, *18*, 2244−2249.

(16) Suman, K.; Joshi, Y. M. Microstructure and Soft Glassy Dynamics of an Aqueous Laponite Dispersion. *Langmuir* **2018**, *34*, 13079−13103.

(17) Choudhury, S. A Highly Reversible Room-Temperature Lithium Metal Battery Based on Cross-Linked Hairy Nanoparticles. In *Rational Design of Nanostructured Polymer Electrolytes and Solid−Liquid Interphases for Lithium Batteries*; Choudhury, S., Ed.; Springer International Publishing: Cham, 2019; pp 35−57.

(18) Agrawal, A.; Choudhury, S.; Archer, L. A. A highly conductive, non-flammable polymer-nanoparticle hybrid electrolyte. *RSC Adv.* **2015**, *5*, 20800−20809.

(19) Choudhury, S.; Agrawal, A.; Wei, S. Y.; Jeng, E.; Archer, L. A. Hybrid Hairy Nanoparticle Electrolytes Stabilizing Lithium Metal Batteries. *Chem. Mater.* **2016**, *28*, 2147−2157.

(20) Kim, M. S.; Ma, L.; Choudhury, S.; Moganty, S. S.; Wei, S.; Archer, L. A. Fabricating multifunctional nanoparticle membranes by a fast layer-by-layer Langmuir−Blodgett process: application in lithium−sulfur batteries. *J. Mater. Chem. A* **2016**, *4*, 14709−14719.

(21) Ragouilliaux, A.; Ovarlez, G.; Shahidzadeh-Bonn, N.; Herzhaft, B.; Palermo, T.; Coussot, P. Transition from a simple yield-stress fluid to a thixotropic material. *Phys. Rev. E* **2007**, *76*, No. 051408.

(22) Pignon, F.; Magnin, A.; Piau, J. M. Thixotropic colloidal suspensions and flow curves with minimum: Identification of flow regimes and rheometric consequences. *J. Rheol.* **1996**, *40*, 573−587.

(23) Sollich, P.; Lequeux, F.; Hébraud, P.; Cates, M. E. Rheology of Soft Glassy Materials. *Phys. Rev. Lett.* **1997**, *78*, No. 2020.

(24) Sollich, P. Rheological constitutive equation for a model of soft glassy materials. *Phys. Rev. E* **1998**, *58*, No. 738.

(25) Agarwal, P.; Qi, H. B.; Archer, L. A. The Ages in a Self-Suspended Nanoparticle Liquid. *Nano Lett.* **2010**, *10*, 111−115.

(26) Agrawal, A.; Wenning, B. M.; Choudhury, S.; Archer, L. A. Interactions, Structure, and Dynamics of Polymer-Tethered Nanoparticle Blends. *Langmuir* **2016**, *32*, 8698−8708.

(27) Agrawal, A.; Yu, H. Y.; Sagar, A.; Choudhury, S.; Archer, L. A. Molecular Origins of Temperature-Induced Jamming in Self-Suspended Hairy Nanoparticles. *Macromolecules* **2016**, *49*, 8738−8747.

(28) Agrawal, A.; Yu, H.-Y.; Srivastava, S.; Choudhury, S.; Narayanan, S.; Archer, L. A. Dynamics and yielding of binary self-suspended nanoparticle fluids. *Soft Matter* **2015**, *11*, 5224−5234.

(29) Choudhury, S.; Agrawal, A.; Kim, S. A.; Archer, L. A. Self-Suspended Suspensions of Covalently Grafted Hairy Nanoparticles. *Langmuir* **2015**, *31*, 3222−3231.

(30) Srivastava, S.; Choudhury, S.; Agrawal, A.; Archer, L. A. Self-suspended polymer grafted nanoparticles. *Curr. Opin. Chem. Eng.* **2017**, *16*, 92−101.
(31) Agarwal, P.; Archer, L. A. Strain-accelerated dynamics of soft colloidal glasses. *Phys. Rev. E* **2011**, *83*, No. 041402.
(32) Rodriguez, R.; Herrera, R.; Bourlinos, A. B.; Li, R.; Amassian, A.; Archer, L. A.; Giannelis, E. P. The synthesis and properties of nanoscale ionic materials. *Appl. Organomet. Chem.* **2010**, *24*, 581−589.
(33) Liu, X.; Abel, B. A.; Zhao, Q.; Li, S.; Choudhury, S.; Zheng, J.; Archer, L. A. Microscopic Origins of Caging and Equilibration of Self-Suspended Hairy Nanoparticles. *Macromolecules* **2019**, *52*, 8187−8196.
(34) Lin, N. Y. C.; Guy, B. M.; Hermes, M.; Ness, C.; Sun, J.; Poon, W. C. K.; Cohen, I. Hydrodynamic and Contact Contributions to Continuous Shear Thickening in Colloidal Suspensions. *Phys. Rev. Lett.* **2015**, *115*, No. 228304.
(35) Kim, S. A.; Archer, L. A. Hierarchical Structure in Semicrystalline Polymers Tethered toNanospheres. *Macromolecules* **2014**, *47*, 687−694.
(36) Pielichowski, K.; Flejtuch, K. Differential scanning calorimetry studies on poly(ethylene glycol) with different molecular weights for thermal energy storage materials. *Polym. Adv. Technol.* **2002**, *13*, 690−696.
(37) Srivastava, S.; Shin, J. H.; Archer, L. A. Structure and rheology of nanoparticle-polymer suspensions. *Soft Matter* **2012**, *8*, 4097−4108.
(38) Glatter, O.; Kratky, O. *Small Angle X-Ray Scattering*; Academic Press: London; New York, 1982; p 515.
(39) Li, T.; Senesi, A. J.; Lee, B. Small Angle X-ray Scattering for Nanoparticle Research. *Chem. Rev.* **2016**, *116*, 11128−11180.
(40) Agarwal, P.; Srivastava, S.; Archer, L. A. Thermal Jamming of a Colloidal Glass. *Phys. Rev. Lett.* **2011**, *107*, No. 268302.
(41) Matsuura, H.; Miyazawa, T. Vibrational analysis of molten poly(ethylene glycol). *J. Polym. Sci., Part A-2: Polym. Phys.* **1969**, *7*, 1735−1744.
(42) Ford, J. L.; Stewart, A. F.; Dubois, J.-L. The properties of solid dispersions of indomethacin or phenylbutazone in polyethylene glycol. *Int. J. Pharm.* **1986**, *28*, 11−22.
(43) Maxfield, J.; Shepherd, I. W. Conformation of poly(ethylene oxide) in the solid state, melt and solution measured by Raman scattering. *Polymer* **1975**, *16*, 505−509.
(44) Yu, H.-Y.; Srivastava, S.; Archer, L. A.; Koch, D. L. Structure factor of blends of solvent-free nanoparticle−organic hybrid materials: density-functional theory and small angle X-ray scattering. *Soft Matter* **2014**, *10*, 9120−9135.
(45) Yu, H. Y.; Koch, D. L. Structure of Solvent-Free Nanoparticle-Organic Hybrid Materials. *Langmuir* **2010**, *26*, 16801−16811.
(46) Srivastava, S.; Archer, L. A.; Narayanan, S. Structure and Transport Anomalies in Soft Colloids. *Phys. Rev. Lett.* **2013**, *110*, No. 148302.
(47) Chremos, A.; Douglas, J. F. Particle localization and hyperuniformity of polymer-grafted nanoparticle materials. *Ann. Phys.* **2017**, *529*, No. 1600342.
(48) Kim, D.; Srivastava, S.; Narayanan, S.; Archer, L. A. Polymer nanocomposites: polymer and particle dynamics. *Soft Matter* **2012**, *8*, 10813−10818.
(49) Seth, J. R.; Mohan, L.; Locatelli-Champagne, C.; Cloitre, M.; Bonnecaze, R. T. A micromechanical model to predict the flow of soft particle glasses. *Nat. Mater.* **2011**, *10*, 838−843.
(50) Erwin, B. M.; Cloitre, M.; Gauthier, M.; Vlassopoulos, D. Dynamics and rheology of colloidal star polymers. *Soft Matter* **2010**, *6*, 2825−2833.
(51) Tadmor, R.; Janik, J.; Klein, J.; Fetters, L. J. Sliding Friction with Polymer Brushes. *Phys. Rev. Lett.* **2003**, *91*, No. 115503.
(52) Fielding, S. M. Shear banding in soft glassy materials. *Rep. Prog. Phys.* **2014**, *77*, No. 102601.
(53) Beris, A. N.; Stiakakis, E.; Vlassopoulos, D. A thermodynamically consistent model for the thixotropic behavior of concentrated star polymer suspensions. *J. Non-Newtonian Fluid Mech.* **2008**, *152*, 76−85.
(54) Griffiths, P. R.; De Haseth, J. A. *Fourier Transform Infrared Spectrometry*; John Wiley & Sons, 2007; Vol. *171*.
(55) Hiemenz, P. C.; Lodge, T. P. *Polymer Chemistry*; CRC Press, 2007.

https://dx.doi.org/10.1021/acs.macromol.0c01448
Macromolecules 2021, 54, 426−439